Journal of Magnetism and Magnetic Materials 354 (2014) 125–135

Contents lists available at ScienceDirect

Journal of Magnetism and Magnetic Materials

journal homepage: www.elsevier.com/locate/jmmm

Shape-induced anisotropy in antiferromagnetic nanoparticles

O. Gomonay *, S. Kondovych, V. Loktev

National Technical University of Ukraine "KPI", ave Peremogy, 37, 03056 Kyiv, Ukraine

ARTICLE INFO

Article history:
Received 20 August 2013
Received in revised form
25 October 2013
Available online 11 November 2013

Keywords:
Antiferromagnet
Domain structure
Nanoparticle
Shape effect

ABSTRACT

High fraction of the surface atoms considerably enhances the influence of size and shape on the magnetic and electronic properties of nanoparticles. Shape effects in ferromagnetic nanoparticles are well understood and allow us to set and control the parameters of a sample that affect its magnetic anisotropy during production. In the present paper we study the shape effects in the other widely used magnetic materials – antiferromagnets, – which possess vanishingly small or zero macroscopic magnetization. We take into account the difference between the surface and bulk magnetic anisotropy of a nanoparticle and show that the effective magnetic anisotropy depends on the particle shape and crystallographic orientation of its faces. The corresponding shape-induced contribution to the magnetic anisotropy energy is proportional to the particle volume, depends on magnetostriction, and can cause formation of equilibrium domain structure. Crystallographic orientation of the nanoparticle surface determines the type of domain structure. The proposed model allows us to predict the magnetic properties of antiferromagnetic nanoparticles depending on their shape and treatment.

1. Introduction

Magnetic nanoparticles (NP) are widely used as constitutive elements for the information technology (e.g. memory cells, spin valves, magnetic field controllers etc.). To drive and control the magnetic state of a particle and values of critical fields and currents, we can use not only internal properties of magnetic material, but also shape and size of the sample. As for ferromagnetic (FM) particles, shape effects allow us to tailor the effective magnetic anisotropy and critical field values during production.

On the other hand, nowadays technologies use antiferromagnetic (AFM) nanoparticles along with (or sometimes instead of) FM ones. Experiments with AFM particles show that the reduction of size to tens of nanometres leads to noticeable changes of properties compared to the bulk samples: an increase of lattice parameters in the magnetically ordered phase [1–3]; an increase of the magnetic anisotropy [4]; a pronounced decrease of AFMR frequency [5]. Some of the finite size effects could be caused by the shape and faces orientations of nanoparticle. For example, according to the Néel predictions [6,7], small AFM particles exhibit uncompensated magnetic moment with the size- and shape-dependent value [8,9]. Recent experiments with rather large (100–500 nm size) AFM particles [10–12] discovered the shape effects similar to the shape-induced phenomena in FM materials: (i) switching of AFM vector from crystallographic to particle easy-axis with an increase of aspect ratio; (ii) correlation between the type of domain structure and such parameters as aspect ratio of the sample and orientation of faces.

However, the mechanism of the finite-size and shape effects in AFM nanoparticles is still an open issue.

Shape effects in AFM particles could, in principle, originate from a weak ferromagnetic moment [13] thus reducing the difference between AFM and FM systems to quantitative one. On the other hand, AFMs show some peculiar features (like exchange enhancement, gap in the magnon spectra, coupling to the external magnetic field) that have no counterparts in FMs.

Understanding the mechanisms of the shape effects specific to AFM ordered systems is crucial for optimizing and finetuning the properties of AFM-based devices and clarifying the fundamental questions whether the shape effects reside in AFM with vanishingly small macroscopic magnetization, and which of peculiar AFM properties might depend on the particle shape. For this purpose we investigate the finite-size and shape effects in AFM particles, regardless of their macroscopic magnetization, combining two previously shown statements: (i) the shape effects in AFM materials may originate from the long-range fields of "magnetoelastic" charges due to spontaneous magnetostriction below the Néel temperature (so-called destressing fields) [14]; (ii) "magnetoelastic" charges may arise from the surface magnetic anisotropy [15]. We consider the particles with the characteristic size below the several critical lengths of monodomainization (which, for convenience, are referred to as "nanoparticles" though their dimensions could also fall into submicron–micron range).

* Corresponding author. Tel.: +380 44 406 83 55.
E-mail addresses: helen.gomonay@gmail.com, homo@pti.kpi.ua (O. Gomonay).

0304-8853/$ - see front matter © 2013 Elsevier B.V. All rights reserved.
http://dx.doi.org/10.1016/j.jmmm.2013.11.003

The basic idea is to consider a priori the surface and bulk properties as different: to distinguish the constants of surface and bulk magnetic anisotropy and, as a consequence, equilibrium orientation of AFM vectors at the surface and in the bulk. Up to our knowledge, M.I. Kaganov [16] was first who pointed out the role of the surface magnetic anisotropy effects on spin-flop transitions in magnetic materials, considering the magnetic moment at the surface as an additional parameter. This idea was then generalized to account for surface exchange interactions and was applied to description of various inhomogeneous states at a nanoscale range, including vortices and twisted phases [17–19]. In our work we further develop this approach introducing into model the magnetoelastic coupling, which, as we believe, noticeably affects the properties of the nanosized AFM particle. We show that due to the long-range nature of magnetoelastic and elastic forces, the surface anisotropy contributes to the magnetic energy of the sample. This contribution is proportional to the particle volume, depends on the aspect ratio and crystallographic orientation of the sample faces, and affects equilibrium (single- and multi-domain) state of AFM nanoparticle. The proposed approach requires consistent description of the magnetic and elastic subsystems of AFM particles and thus differs from the well-known formalism for the FM [20].

2. Model

To describe the equilibrium magnetic state of a NP we need to introduce at least three additional (in comparison with bulk samples) parameters that characterize: (i) shape, (ii) size, and (iii) orientation of sample faces.

We consider a thin flat rectangular particle (thickness $h \ll b < a$, Fig. 1), typical for experimental studies (see, e.g., [12]). The thickness h of a particle is, however, large enough to ensure an AFM ordering (i.e. significantly larger than the magnetic correlation length).

The sample surface (see Fig. 1b) consists of four faces with the normal vectors $\mathbf{n}_j = (\cos\psi_j, \sin\psi_j)$, $j = 1, \ldots, 4$ (x, y are parallel to crystallographic axes). We disregard the upper and lower faces (z=Z=$const$) as they do not contribute to the effects discussed below. Equations that define the surface are ($Z \in [0, h]$, X, Y are parallel to the particle edges):

$$\begin{aligned} &X = a/2, \quad Y \in [-b/2, b/2], \quad \mathbf{n}_1 = (1,0), \quad \psi_1 = \psi, \\ &Y = b/2, \quad X \in [-a/2, a/2], \quad \mathbf{n}_2 = (0,1), \quad \psi_2 = \psi + \pi/2, \\ &X = -a/2, \quad Y \in [-b/2, b/2], \quad \mathbf{n}_3 = (-1,0), \quad \psi_3 = \psi + \pi, \\ &Y = -b/2, \quad X \in [-a/2, a/2], \quad \mathbf{n}_4 = (0,-1), \quad \psi_4 = \psi + 3\pi/2. \end{aligned} \tag{1}$$

For such a model, the additional external (in thermodynamic sense) parameters of the NP are: (i) aspect ratio a/b (defines the shape), (ii) width b (defines characteristic size), and (iii) angle ψ (defines the orientation of the surfaces).

We consider a typical collinear AFM with two equivalent sublattices $\mathbf{M}_1$ and $\mathbf{M}_2$; the Néel (or AFM) vector $\mathbf{L} = \mathbf{M}_1 - \mathbf{M}_2$ plays a role of the order parameter. Far below the critical point the magnitude of the AFM vector is fixed (we assume $|\mathbf{L}| = 1$).

To obtain equilibrium distribution $\mathbf{L}(\mathbf{r})$ for the NP of given shape and size, we minimize the total energy W which includes several terms of different nature. First of all, we may consider the surface as a separate magnetic phase [21–23] with a small but finite thickness δ_{sur} (narrow peripheral region S of thickness δ_{sur} in Fig. 2) and thus distinguish the bulk, W_{bulk}, and the surface, W_{sur}, contributions:

$$W = W_{bulk} + W_{sur}. \tag{2}$$

Then, we can also distinguish different contributions to the bulk energy, W_{bulk}, the most important are those that describe the magnetic anisotropy, w_{anis}, exchange, w_{exch}, and magnetoelastic, w_{m-e} coupling. We assume that the bulk magnetic anisotropy corresponds to tetragonal symmetry with two equivalent easy directions in the NP plane (x or y in Fig. 1b) and model respective contribution to the energy density as follows:

$$w_{anis} = \tfrac{1}{2} K_{\parallel} L_z^2 - K_{\perp}(L_x^4 + L_y^4), \tag{3}$$

where $K_{\parallel} \gg K_{\perp} > 0$ are the phenomenologic anisotropy constants.

Exchange interactions (responsible for inhomogeneous distribution of the Néel vector inside the sample) give rise to a gradient term

$$w_{exch} = \tfrac{1}{2}\alpha(\nabla \mathbf{L})^2, \tag{4}$$

where α is a phenomenological constant. Competition between the exchange coupling (4) and magnetic anisotropy (3) defines the characteristic size ξ_{DW} of the domain wall (DW): $\xi_{DW} = (1/2)\sqrt{\alpha/K_{\perp}}$.

Magnetoelastic coupling in AFM materials can be pronounced (compared with FM ones) due to the presence of strong crystal field and, as a result, strong spin–orbit coupling (like in oxides $LaFeO_3$ or NiO). In the simplest case of the elastically isotropic

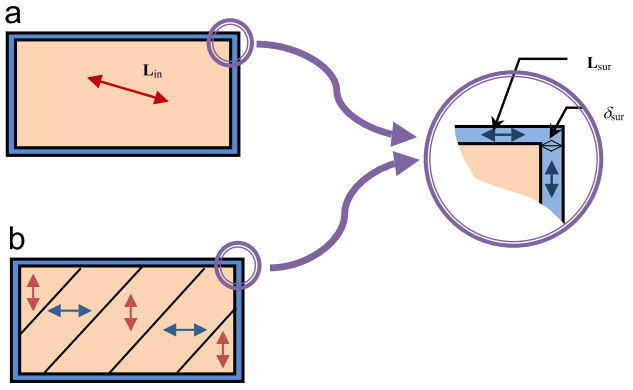

Fig. 2. Space distribution of AFM vector (arrows) in a single domain (a) and multidomain (b) states.

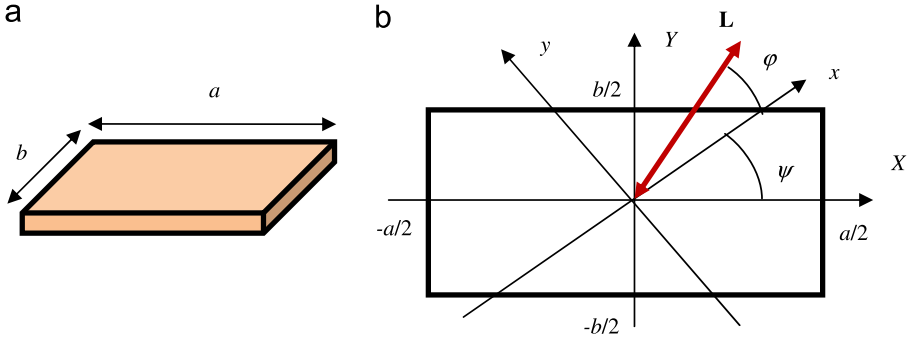

Fig. 1. Sample (a) and orientation of the Néel vector **L** (b) with respect to crystal axes (x,y) and sample edges (X,Y).

material, the density of magnetoelastic energy is:

$$w_{m-e} = \lambda_{iso}\mathbf{L}^2 \mathrm{Tr}\hat{u} + 2\lambda_{anis}[(\mathbf{L}\otimes\mathbf{L} - \tfrac{1}{3}\hat{I})(\hat{u} - \tfrac{1}{3}\hat{I}\ \mathrm{Tr}\ \hat{u})], \quad (5)$$

where $\hat{u}$ is the strain tensor, $\hat{I}$ is the identity matrix, constants λ_{iso} and λ_{anis} describe isotropic and shear magnetostriction, respectively.

Final expression for the bulk energy is thus given by

$$W_{bulk} = \int_V (w_{anis} + w_{exch} + w_{m-e} + w_{elas})\, dV, \quad (6)$$

where w_{elas} is the elastic energy density (see, e.g. [24]), $V=abh$ is the NP volume, all other terms are defined above.

At last, let us focus on the magnetic surface energy W_{sur} which is of crucial importance for our model and needs special discussion. Experiments with the nanoscale AFM particles reveal a significant difference between the magnetic ordering and hence the magnetic properties of the surface from those of the bulk. In particular, depending on the material, treatment, and other technological factors, the NP surface may lack the long-range magnetic structure (paramagnetic or spin glass [23,25]), or may have different type of ordering (e.g. multi- vs. two-sublatteral in the bulk [26]), or different easy axis/axes. We consider the last case and assume, for the sake of simplicity, that the easy magnetic axis at the surface is perpendicular to the normal $\mathbf{n}$; then, expression for the magnetic surface energy takes the form:

$$W_{sur} = K_{sur}\oint_s (\mathbf{Ln})^2\, dS = K_{sur}\sum_{j=1}^{4}\int_{S_j}(\mathbf{Ln}_j)^2\, dS, \quad (7)$$

where $K_{sur} > 0$ is a phenomenological constant. W_{sur} obviously depends on orientation of edges: angles ψ_j, or, equivalently, vectors $\mathbf{n}_j$ (see (1)).

It is instructive to compare the specific surface magnetic anisotropy K_{sur}/δ_{sur} with the magnetic anisotropy constant $K_\perp$: they have the same order of value ($K_{sur}/\delta_{sur} \propto K_\perp$), if the broken exchange bonds play the main role in formation of the surface properties; while in the case of dominating dipole-dipole interactions K_{sur}/δ_{sur} can be much greater than $K_\perp$ [13].

It should be stresses, that, in principle, all introduced phenomenological constants fall into two categories: internal [27] (indexed "in") and superficial (indexed "sur"); interactions of both types can contribute to the shape effects. However, in our model we distinguish only between the magnetic constants K_{sur}/δ_{sur} and $K_\perp$, taking this difference as the most important.

The expression (2) for the NP energy is the functional over the field variables $\mathbf{L}(\mathbf{r})$ (the AFM vector) and $\mathbf{u}(\mathbf{r})$ (the displacement vector). We reduce the number of independent variables to three assuming that: (i) vector $\mathbf{L}$ lies within the xy plane and can be parametrized by a single angle φ (see Fig. 1b because of a strong easy-plane anisotropy ($K_\parallel \gg K_\perp$); (ii) strain component u_{zz} in a rather thin plate ($h \gg a, b$) can be considered as homogeneous and thus can be excluded from consideration (see [24]). The standard minimum conditions generate the set of differential equations for one magnetic, $\varphi(\mathbf{r})$, and two elastic, $u_x(\mathbf{r})$, $u_y(\mathbf{r})$ variables in the bulk:

$$-\alpha\Delta\varphi + K_\perp\ \sin\ 4\varphi + 2\lambda_{anis}[-(u_{xx}-u_{yy})\ \sin\ 2\varphi + 2u_{xy}\ \cos\ 2\varphi] = 0, \quad (8)$$

$$\Delta u_x + \nu_{eff}\nabla_x\ \mathrm{div}\ \mathbf{u} = -(\lambda_{anis}/\mu)[\nabla_x\ \cos\ 2\varphi + \nabla_y\ \sin\ 2\varphi], \quad (9)$$

$$\Delta u_y + \nu_{eff}\nabla_y\ \mathrm{div}\ \mathbf{u} = -(\lambda_{anis}/\mu)[\nabla_x\ \sin\ 2\varphi - \nabla_y\ \cos\ 2\varphi]. \quad (10)$$

Here, operators Δ and div are two-dimensional, $\nu_{eff} \equiv (1+\nu)/(1-\nu)$ is the effective Poisson ratio (instead of 3-dimensional ν [24]), μ is the shear modulus.

Equations for the AFM vector at the j-th face (variables $\varphi_{sur}^{(j)}$, see (1))

$$-K_{sur}\ \sin\ 2(\varphi_{sur}^{(j)} + \psi_j) + \alpha(\mathbf{n}_j\nabla)\varphi_{sur}^{(j)} = 0 \quad (11)$$

could be considered as the boundary conditions. They differ from the standard boundary conditions for AFMs (see, e.g., [28,29]) due to the presence of the additional surface term with K_{sur}.

In the limit $K_{sur}\to 0$ the solutions of Eqs. (9), (10), (11) are well known: the AFM vector $\mathbf{L}(\mathbf{r}) = const$ lies along one of the easy axes ($\varphi_{in} = 0$ or $\pi/2$), the displacement vector $\mathbf{u}(\mathbf{r})$ generates the homogeneous field of the magnetically-induced strain:

$$u_{xx}^{(0)} - u_{yy}^{(0)} = -\frac{\lambda_{anis}}{\mu}\ \cos\ 2\varphi_{in}, \quad u_{xy}^{(0)} = -\frac{\lambda_{anis}}{2\mu}\ \sin\ 2\varphi_{in}. \quad (12)$$

In the massive (infinite) samples the spontaneous striction (12) causes magnetoelastic gap in the spin-wave spectrum (in assumption of "frozen" lattice), but does not affect the equilibrium orientation of the AFM vector (all the magnetostrictive terms in (8) cancel out, eliminating the shape effect).

For the finite-size samples with nonzero surface anisotropy ($K_{sur} \neq 0$) the easy direction at least in some near-surface regions unavoidably differs from that in the bulk and so, the spatial distribution of the AFM vector should be non-uniform. As a result, the sources of the displacement field – the nonzero gradient terms, or "*magnetoelastic charges*" – appear in the r.h.s of Eqs. (9) and (10). In the following section we discuss this issue in more detail.

3. Shape-induced anisotropy

The consistent theory of shape effects in AFMs should account for the long-range elastic and magnetoelastic interactions and thus should rest upon the complete set of Eqs. (8)–(10). However, the displacement field $\mathbf{u}(\mathbf{r})$ can be formally excluded from consideration once the Green tensor $G_{jk}(\mathbf{r},\mathbf{r}')$ for Eqs. (9) and (10) is known (see Appendix A). In this case the spatial distribution of the AFM vector $\mathbf{L}(\mathbf{r})$ should minimize the energy functional

$$W[\mathbf{L}(\mathbf{r})] = \int_V (w_{mag} + w_{exch})\, dV + W_{sur} + W_{add}, \quad (13)$$

which includes the additional term of magnetoelastic nature:

$$W_{add} = \frac{2\lambda_{anis}^2}{\mu}\int_V\int_V \nabla_m[L_j(\mathbf{r})L_m(\mathbf{r})]G_{kj}(\mathbf{r},\mathbf{r}')\nabla_l'[L_k(\mathbf{r}')L_l(\mathbf{r}')]\, dV\, dV' + \frac{2\lambda_{anis}^2}{\mu}\oint_s\oint_s L_j(\mathbf{r}_{sur})L_m(\mathbf{r}_{sur})G_{kj}(\mathbf{r}_{sur},\mathbf{r}_{sur}')L_k(\mathbf{r}_{sur}')L_l(\mathbf{r}_{sur}')\, dS_m\, dS_l'. \quad (14)$$

Analysis of the Exp. (14) shows that any inhomogeneous distribution $\mathbf{L}(\mathbf{r})$ gives nonzero, generally positive contribution to energy W_{add}. Due to the "Coulomb-like" nature of the elastic forces ($G_{jk}(\mathbf{r},\mathbf{r}') \propto 1/|\mathbf{r}-\mathbf{r}'|$) this contribution scales as sample volume V. In addition, nonlocality of the W_{add} term turns Eqs. (8) to integro-differential ones and thus complicates the problem.

In the present paper we propose the simplified approach to solve Eqs. (8)–(10) using the following peculiar features of antiferromagnets.

First, we consider the magnetostriction of AFMs as a secondary order parameter which means that in the thermodynamic limit (in neglection of boundary conditions) the homogeneous spontaneous strains (12) preserve the symmetry of the magnetically ordered state and orientation of the easy axis. In addition, though usually the magnetoelastic energy is comparable (up to the order of value) to the 4-th order magnetic anisotropy (i.e. to $K_\perp$ constant), it can be much less than the uniaxial magnetic anisotropy. Thus, assuming strong uniaxial surface anisotropy $K_{sur} \gg K_\perp\delta_{sur}$, we can disregard the influence of magnetoelastic strains on equilibrium orientation of

AFM vector at the surface. However, this assumption does not restrict the relation between K_{sur} and the characteristic DW energy σ_{DW}, because $\sigma_{DW} \propto \sqrt{K_\perp J} a_{lat} \gg K_\perp \delta_{sur}$ (where $J \gg K_\perp$ characterizes the exchange coupling, a_{lat} is the lattice constant, and we used the following relations: $\alpha \propto J a_{lat}^2$, $\delta_{sur} \propto a_{lat}$).

Second, we propose the following hierarchy of characteristic length scales: the width of magnetic inhomogeneity is much less than the sample size, $\xi_{DW} \ll a, b$, but much greater than interatomic distance, $\xi_{DW} \gg a_{lat}$ (due to exchange enhancement); the width of elastic inhomogeneity has interatomic scale and thus is much less than ξ_{DW}. Note, that the value of ξ_{DW} in nanoparticles with the large fraction of the surface atoms can be much smaller than that for the bulk samples due to variation of magnetoelastic and exchange coupling (see, e.g. [30]). Thus, inequality $\xi_{DW} \ll a, b$ keeps true in a wide range of the sample dimensions down to tens of nanometers (below this range applicability of the continual model is questionable).

Thus, within the above approximations, equilibrium orientation of the AFM vector at the surface results mainly from competition of the magnetic interactions: surface magnetic anisotropy and inhomogeneous exchange coupling, once the bulk vector $\mathbf{L}_{in}$ is fixed. Orientation of $\mathbf{L}_{in}$, in turn, is defined by interplay between the bulk magnetic anisotropy and magnetostrictive contribution induced by spatial rotation of AFM vector in the thin ($\propto \xi_{DW}$) near-surface region (see Fig. 3). So, the effective shape-induced magnetic anisotropy and equilibrium distribution of AFM vector could be determined self-consistently according to the following procedure: (i) to calculate $\mathbf{L}_{sur}$ starting from some (initially unknown) "seed" distribution of the AFM vector $\mathbf{L}_{in}$ in the NP bulk; (ii) to substitute thus defined seed distribution into equations for the displacement vector and to determine the corresponding field sources (magnetoelastic charges); (iii) to calculate charge-induced average strains whose contribution into free energy is proportional to the sample volume; (iv) to define the effective magnetic anisotropy which accounts for the average strains and calculate $\mathbf{L}_{in}$.

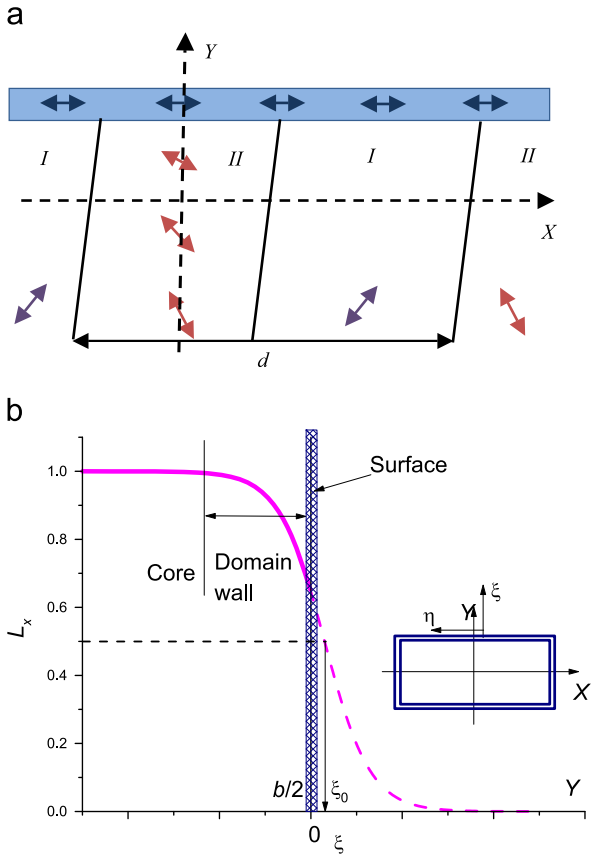

Fig. 3. Distribution of the Néel vector in the vicinity of $Y=b/2$ face, multidomain state. (a) Periodic (period d) domain structure, double arrows indicate orientation of AFM vectors inside domains and in the near-surface region (shaded horizontal stripe). (b) Space dependence of $L_x(\xi)$ (solid line) calculated from (15) provided that $\varphi_{in}=0$. The horizontal line defines the center ξ_0 of a virtual full domain wall (dotted line). Shaded vertical bar indicates the position of surface region. Direction of DW normal coincides with the axis ξ of the local coordinate system (inset).

Note, that the form of the seed distribution (and hence the free variable of the structure) is different for a single- and a multidomain states. In the first case $\mathbf{L}_{in}$ is homogeneous within the bulk but can deflect from the magnetic easy axis, so, φ_{in} is the appropriate free variable. In the second case we assume, in analogy with FM, that AFM vector within each of the domains is fixed and parallel to one of two equivalent easy axes; then, free variable coincides with the fraction of type-I (or type-II) domains.

3.1. Seed distribution and magnetoelastic charges

In the simplest case of a single-domain state (Fig. 2a), there are two homogeneous regions: the "shell" (of the thickness δ_{sur}) and the core. An equilibrium value φ_{in} inside the core is fixed, constant (as $\Delta\varphi_{in}=0$), but unknown (in some cases discussed below $\varphi_{in}=0$ or $\pi/2$ that corresponds to one of the easy axes). We calculate the value $\varphi_{sur}^{(j)}$ at the surface from Eq. (11) with account of the standard expression for the domain wall profile:

$$\sin 2(\varphi(\xi)-\varphi_{in}) = 2\xi_{DW}\frac{d\varphi}{d\xi} = \frac{1}{\cosh((\xi-\xi_0)/\xi_{DW})}. \tag{15}$$

Face normals generate the set of variables $\xi=(\pm X-a/2)$, $(\pm Y-b/2)$ of the local coordinate system (see the inset in Fig. 3b). Position ξ_0 of the DW center is calculated from the boundary conditions (see below). In (15) we neglect the possible difference between the DW width $\xi_{DW}=(1/2)\sqrt{\alpha/K_\perp}$ in the near-surface region and in the core.

Substituting (15) in (11), we obtain the following equation for $\varphi_{sur}^{(j)}$:

$$\tan 2\varphi_{sur}^{(j)} = \frac{K_{sur}\sin 2\psi_j + \sigma_{DW}\sin 2\varphi_{in}}{\sigma_{DW}\cos 2\varphi_{in} - K_{sur}\cos 2\psi_j}, \tag{16}$$

where $\sigma_{DW}=\sqrt{\alpha K_\perp}=2\xi_{DW}K_\perp$ is the characteristic energy of the domain wall. The values $\varphi_{sur}^{(j)}$ at the opposite faces coincide: $\varphi_{sur}^{(1)}=\varphi_{sur}^{(3)}$, $\varphi_{sur}^{(2)}=\varphi_{sur}^{(4)}$ (see (1)).

Analysis of Exp. (16) shows that the AFM vector at the surface can be either parallel to the edge: $\varphi_{sur}^{(j)}=\psi_j$, as shown in Fig. 2 (in the limit of large surface anisotropy, $K_{sur} \gg \sigma_{DW}$), or coincide with the bulk AFM vector: $\varphi_{sur}^{(j)}=\varphi_{in}$ (for the vanishing surface energy, $K_{sur} \ll \sigma_{DW}$). In the last case the surface influence and, correspondingly, shape effects disappear.

Note that the surface DW is "incomplete": in general, DW center is located outside the sample (see Fig. 3b) and its coordinate $\xi_0^{(j)}$ depends on the surface anisotropy

$$\xi_0^{(j)} = \xi_{DW}\sinh^{-1}\frac{K_{sur}\sin 2\psi_j + \sigma_{DW}\sin 2\varphi_{in}}{\sigma_{DW}\cos 2\varphi_{in} - K_{sur}\cos 2\psi_j}. \tag{17}$$

In a single-domain nanoparticle the AFM vector rotates from $\mathbf{L}_{sur}$ to $\mathbf{L}_{in}$ in a narrow, almost zero-width ($\leq \xi_{DW} \ll a, b$) region and so, we can model the spatial dependence of $\mathbf{L}(\mathbf{r})$ with a step-like function. Within this approximation, r.h.s. of Eqs. (9) and (10) are nontrivial only at the surface; this fact makes it possible to use a homogeneous form of these equations for the bulk region of the NP:

$$\Delta\mathbf{u} + \nu_{eff}\nabla \mathrm{div}\,\mathbf{u} = 0 \tag{18}$$

with the following boundary conditions for the displacement vector:

$$(\mathbf{n}\cdot\nabla)\mathbf{u}_{\rm sur}+\nu_{\rm eff}\mathbf{n}\ \mathrm{div}\ \mathbf{u}_{\rm sur}=\mathbf{n}\hat{Q}^{\rm m-e}. \tag{19}$$

In (19) we introduced the tensor of magnetoelastic charges as follows:

$$\hat{Q}^{\rm m-e}\equiv-\frac{\lambda_{\rm anis}}{\mu}[\mathbf{L}_{\rm sur}\otimes\mathbf{L}_{\rm sur}-\mathbf{L}_{\rm in}\otimes\mathbf{L}_{\rm in}]. \tag{20}$$

For a rectangular-shaped sample the charges at the opposite edges coincide: $\hat{Q}^{\rm m-e}(\mathbf{n}_1)=\hat{Q}^{\rm m-e}(\mathbf{n}_3)$, $\hat{Q}^{\rm m-e}(\mathbf{n}_2)=\hat{Q}^{\rm m-e}(\mathbf{n}_4)$. We can express all the components of the $\hat{Q}^{\rm m-e}$ tensor in terms of two nontrivial combinations, $Q_1^{\rm m-e}\equiv Q_{XX}^{\rm m-e}-Q_{YY}^{\rm m-e}$ and $Q_2^{\rm m-e}\equiv 2Q_{XY}^{\rm m-e}$ (in X, Y coordinates).

From definition (20) and the relations (16) it follows that

$$Q_1^{\rm m-e}(\mathbf{n}_{1,2})=\frac{\lambda_{\rm anis}}{\mu}\left(\cos\ 2(\varphi_{\rm in}+\psi)-\frac{\sigma_{DW}\ \cos\ 2(\varphi_{\rm in}+\psi)\mp K_{\rm sur}}{\sqrt{K_{\rm sur}^2\mp 2K_{\rm sur}\sigma_{DW}\ \cos\ 2(\varphi_{\rm in}+\psi)+\sigma_{DW}^2}}\right), \tag{21}$$

and

$$Q_2^{\rm m-e}(\mathbf{n}_{1,2})=\frac{\lambda_{\rm anis}}{\mu}\sin\ 2(\varphi_{\rm in}+\psi)\left(1-\frac{\sigma_{DW}}{\sqrt{K_{\rm sur}^2\mp 2K_{\rm sur}\sigma_{DW}\ \cos\ 2(\varphi_{\rm in}+\psi)+\sigma_{DW}^2}}\right). \tag{22}$$

Magnetoelastic charges (20) (as well as (21), (22)) are similar to "magnetostatic charges" at the surface of FMs but have another, magnetoelastic, nature (i.e. depend on magnetostriction), and depend on the surface magnetic anisotropy $K_{\rm sur}$. Magnetoelastic charges disappear in the limiting case of small surface anisotropy $K_{\rm sur}\ll\sigma_{DW}$ and reach the maximum possible value when $K_{\rm sur}\gg\sigma_{DW}$ (as illustrated in Fig. 4). Like magnetostatic, magnetoelastic charges depend on the crystallographic orientation of the sample faces and vanish for those parts of the surface where $\mathbf{L}_{\rm in}\parallel\mathbf{L}_{\rm sur}$. From Eqs. (18), (19) it follows that magnetoelastic charges produce *long-range* (decaying as $1/r^2$) elastic fields, which, in turn, lead to the "destressing" effects (similar to "demagnetizing" effects in FMs).

Another way to interpret the formation of magnetoelastic charges presents itself in terms of incompatibility of seed spontaneous deformations at the surface and in the bulk. To this end, sufficient condition for charges to appear stems from the difference between the surface and bulk values of *any* physical quantity: magnetic (e.g. nonmagnetic or paramagnetic surface), magnetoelastic, or elastic (e.g. rigid shell).

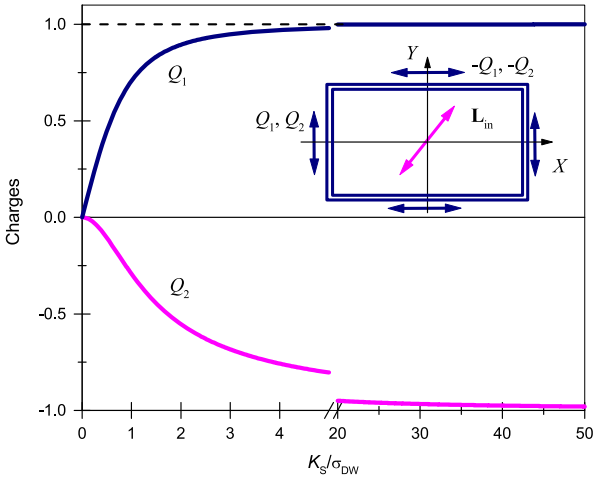

Fig. 4. Magnetoelastic charges $Q^{\rm m-e}$ (in $\lambda_{\rm anis}/\mu$ units) vs. surface constant $K_{\rm sur}$ calculated for single-domain state, $\psi=\pi/4$. Inset shows the charge distribution over the particles edges. Arrows indicate orientation of AFM vector at the surface and in the bulk.

3.2. Average strains and shape-induced anisotropy

At the next, (iii), stage of the algorithm we solve Eqs. (18), (19) for the displacement vector which, in a general case, generates non-uniform field of additional (compared with (12)) elastic deformations. However, the main contribution to the magnetic anisotropy comes from the shear strains averaged over the sample volume (labeled as $\langle\cdots\rangle$) :

$$\langle u_{XX}-u_{YY}\rangle=-\frac{\pi}{1+\nu_{\rm eff}}\Big\{[Q_1^{\rm m-e}(\mathbf{n}_2)+Q_1^{\rm m-e}(\mathbf{n}_1)]\Big[1+\nu_{\rm eff}J_2\Big(\frac{a}{b}\Big)\Big] -J_1\Big(\frac{a}{b}\Big)[Q_1^{\rm m-e}(\mathbf{n}_1)-Q_1^{\rm m-e}(\mathbf{n}_2)]\Big\}, \tag{23}$$

$$2\langle u_{XY}\rangle=-\pi\Big\{[Q_2^{\rm m-e}(\mathbf{n}_2)+Q_2^{\rm m-e}(\mathbf{n}_1)]\Big[1-\frac{\nu_{\rm eff}}{1+\nu_{\rm eff}}J_2\Big(\frac{a}{b}\Big)\Big] -J_1\Big(\frac{a}{b}\Big)[Q_2^{\rm m-e}(\mathbf{n}_1)-Q_2^{\rm m-e}(\mathbf{n}_2)]\Big\}, \tag{24}$$

where $J_1(a/b)$, $J_2(a/b)$ are the dimensionless shape functions of the aspect ratio a/b (see Fig. 5):

$$J_1\Big(\frac{a}{b}\Big)=\frac{2}{\pi}\left[\arctan\frac{a}{b}-\arctan\frac{b}{a}+\frac{a}{4b}\ln\Big(1+\frac{b^2}{a^2}\Big)-\frac{b}{4a}\ln\Big(1+\frac{a^2}{b^2}\Big)\right], \tag{25}$$

$$J_2\Big(\frac{a}{b}\Big)=\frac{4}{\pi}\left[\frac{b}{a}\ln\Big(1+\frac{a^2}{b^2}\Big)+\frac{a}{b}\ln\Big(1+\frac{b^2}{a^2}\Big)\right]. \tag{26}$$

Note that $J_2(a/b)=J_2(b/a)$; $J_1(a/b)=-J_1(b/a)$, so, $J_1(1)=0$ for a square ($a=b$); in the opposite limiting case of high aspect ratio ($a\gg b$) $J_1(\infty)\to 1$, $J_2(\infty)\to 0$.

Substituting Exps. (21), (22), (23), and (24) into Eq. (8) we arrive at the following equation for magnetic variable:

$$K_\perp\ \sin\ 4\varphi_{\rm in}+K_2^{\rm sh}\ \sin\ 2(\varphi_{\rm in}+\psi)+K_4^{\rm sh}\ \sin\ 4(\varphi_{\rm in}+\psi)=0, \tag{27}$$

where we introduce the shape-dependent coefficients $K_2^{\rm sh}$, $K_4^{\rm sh}$, and take into account that $\Delta\varphi=0$. In the limiting (and practically

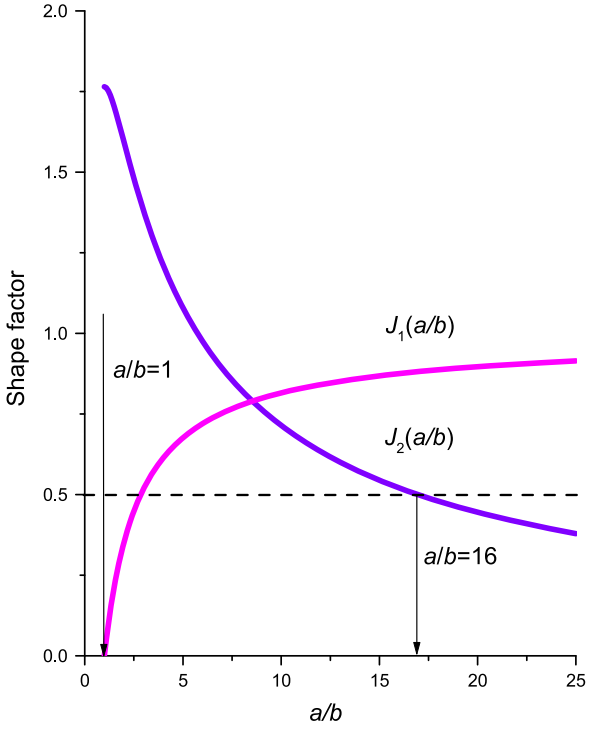

Fig. 5. Form-factors $J_1(a/b)$, $J_2(a/b)$ vs aspect ratio a/b. Arrows show the points where the functions J_1 ($a/b=1$) and $K_4^{\rm sh}$ ($a/b\approx 16$) change the sign.

important) case $K_{sur} \gg \sigma_{DW}$

$$K_2^{sh} = 2\,K^{m-e} J_1\left(\frac{a}{b}\right), \quad K_4^{sh} = K^{m-e}\left[2J_2\left(\frac{a}{b}\right) - 1\right], \quad K^{m-e} \equiv \frac{4\pi\nu_{eff}\lambda_{anis}^2}{(1+\nu_{eff})\mu}. \tag{28}$$

In a general case the coefficients K_2^{sh} and K_4^{sh} depend on the constant K_{sur} of surface magnetic anisotropy and vanish when $K_{sur} \ll \sigma_{DW}$ (see Appendix B).

Eq. (27) for the magnetic variables φ_{in} can be treated as the minimum condition for the effective energy density of the sample

$$w_{eff} \equiv \frac{W_{eff}}{V} = -\frac{1}{4}[K_\perp \cos 4\varphi_{in} + \underline{2K_2^{sh} \cos 2(\varphi_{in}+\psi)} + \underline{K_4^{sh} \cos 4(\varphi_{in}+\psi)}], \tag{29}$$

which, apart from the magnetic anisotropy, includes contributions from magnetoelastic and surface forces (the underlined terms). The last two terms in (29) cause the shape effects in AFM nanoparticle. To illustrate this result we consider some typical cases.

Let the sample edges be parallel to the easy magnetic axes ($\psi = 0$). In this case, as follows from (27) and (29), the term with K_2^{sh} removes degeneracy of states $\varphi_{in} = 0$ and $\varphi_{in} = \pi/2$. This term is equivalent to uniaxial anisotropy, which selects the state with the collinear orientation of AFM vectors at the surface and in the bulk as energetically favorable. This means that the AFM vector is parallel to the long edge of the rectangle: if $a > b$, then $K_2^{sh} > 0$ and $\mathbf{L} \| X$ ($\varphi_{in} = 0$). The second shape-induced term with K_4^{sh} renormalizes the "bare" magnetic anisotropy constant, $K_\perp \to K_\perp + K_4^{sh}$; however, this effect makes no influence on the orientation of the AFM vector. For the square sample ($a = b$) the shape-induced correction has the same sign as $K_\perp$ ($K_4^{sh} > 0$) and thus does not affect equilibrium orientation of the AFM vector. The change of K_4^{sh} sign appears for the samples with large aspect ratio ($a/b \approx 16$, see Fig. 5), where uniaxial anisotropy governs the orientation of the AFM vector, and shape-induced renormalization of $K_\perp$ is insignificant.

The role of the terms with K_4^{sh} becomes noticeable when the faces (edges) of the square ($a = b$) sample are cut at the angle $\psi = \pi/4$ (i.e. along the "hard" magnetic axes). In this case the uniaxial anisotropy vanishes, $K_2^{sh} = 0$ and the effective magnetic anisotropy constant decreases: $K_\perp \to K_\perp - K_4^{sh}$. Assuming that $K_\perp$ and K_4^{sh} have the same (spin-orbit) nature, we conclude that the shape can change the direction of the easy axes (if $K_\perp < K_4^{sh}$) or entirely compensate the 4-th order magnetic anisotropy (if $K_\perp \approx K_4^{sh}$), as it was recently observed in the experiments [12].

4. Multidomain state, destressing energy and critical size

In the multidomain state the seed distribution can, in principle, model the domains and domain boundaries both in the bulk and at the surface. To simplify the problem we assume that distribution of the AFM vector $\mathbf{L}_{sur}(\mathbf{r})$ within each face is homogeneous and $\mathbf{L}_{sur}$ aligns due to the surface anisotropy ($K_{sur} \gg \sigma_{DW}$), as shown in Fig. 3a. In this case, orientation of the AFM vector and, correspondingly, angle φ, can take one of two values within the bulk: $\varphi_{in}^{I} = 0$ or $\varphi_{in}^{II} = \pi/2$ (domains of two types, *I* and *II*). At the surface $\varphi_{sur}^{(1)} = \varphi_{sur}^{(3)}$ and $\varphi_{sur}^{(2)} = \varphi_{sur}^{(4)}$.

Magnetoelastic charges appear near the surface (due to the difference between $\mathbf{L}_{sur}$ and $\mathbf{L}_{in}$) and at the domain walls in the bulk (due to the difference between $\mathbf{L}_{in}^{I}$ and $\mathbf{L}_{in}^{II}$). The total charge of the full domain wall is zero because of the perfect compensation of the charges with opposite signs. So, the field of internal charges decreases rapidly with distance (as $1/r^6$, due to Coulomb-like nature of the "elastic" forces) and can be neglected.

Near-surface domain structure generates two types of the charges, $\hat{Q}_I^{m-e}$ and $\hat{Q}_{II}^{me}$, corresponding to two types of the domains with $\mathbf{L}_{in}^{I}$ and $\mathbf{L}_{in}^{II}$ (see Eq. (20)). Thus, distribution of $\hat{Q}_{I,II}^{m-e}$ is space-dependent. We consider the simplest case of the stripe domain structure (see discussion of possible generalization below) and model it as

$$\hat{Q}^{m-e}(\eta_j) = \langle \hat{Q}_j^{m-e} \rangle + (\hat{Q}_I^{m-e} - \hat{Q}_{II}^{m-e}) f(\eta_j). \tag{30}$$

Here η_j is a local coordinate parallel to the *j*-th edge of the sample (for example, $\eta_2 = -X$ in Fig. 3), and $f(\eta_j)$ is a periodic function with zero mean value: $f(\eta_j + d) = f(\eta_j)$, $\langle f(\eta_j) \rangle = 0$; d is a domain structure period.

In the case of the fine domain structure, $d \ll b, a$, the averaged value $\langle \hat{Q}_j^{me} \rangle$ is independent of j and coincides with that averaged over the particle volume. As in the single-domain state, the effective contribution from the averaged charges to the magnetic energy density is similar to (29):

$$w_{destr} = -\frac{1}{4}\left\{2K_2^{sh}\langle \cos 2(\varphi_{in}+\psi)\rangle + K_4^{sh}[\langle \cos 2(\varphi_{in}+\psi)\rangle^2 - \langle \sin 2(\varphi_{in}+\psi)\rangle^2]\right\}. \tag{31}$$

The term with K_2^{sh} corresponds to the uniaxial shape-induced anisotropy. The second term, with K_4^{sh}, depends nonlinearly on the domain fraction and is analogous to the demagnetization energy of FM. Previously [14] we named this contribution as *destressing* energy, since it determines the equilibrium domain structure in the presence of the external fields (in the defectless samples).

We estimate the energy contribution of the second term in (30) using the analogy between the theory of elasticity and electro-(magneto-)statics: the total field of the alternating charge distribution with zero average decays exponentially into the sample at distances d: $u_j \propto \exp(-|X \pm a/2|/d), \exp(-|Y \pm b/2|/d)$. The corresponding contribution to the total energy density can easily be obtained by analogy with the well-known Kittel expressions for FMs (formulae (54), (63) in [20]):

$$w_{near-sur} = A\mu(\hat{Q}_I^{m-e} - \hat{Q}_{II}^{m-e})^2 \frac{Sd}{V} \tag{32}$$

where A is a factor of the order of unity, S is the surface area.

Comparison of (32) and (31) shows that $w_{near-sur}/w_{destr} \propto d/\ell \ll 1$ (where ℓ is the characteristic size sample). However, contribution $w_{near-sur}$, though small, defines the details of the domain structure (period, number of domains, orientation and shape of DW). Also, as in the case of FM, a period of the equilibrium domain structure is determined by the competition between the energy (32) (which increases with d increase) and the total DW energy density $w_{bound} = \sigma_{DW}\ell S/(Vd)$ (which decreases with d increase). An optimal value d_{opt} (up to an unessential numerical factor) is

$$d_{opt} \approx \sqrt{\frac{\ell\sigma_{DW}}{\mu(\hat{Q}_I^{m-e} - \hat{Q}_{II}^{m-e})^2}}. \tag{33}$$

The period d_{opt} of the domain structure defines the critical NP size ℓ_{cr}, below which the formation of AFM domains becomes energetically unfavorable:

$$\ell_{cr} = d_{opt} = \frac{\sigma_{DW}}{\mu(\hat{Q}_I^{m-e} - \hat{Q}_{II}^{m-e})^2}. \tag{34}$$

Let us compare expressions (33), (34) with the similar expressions for the FM samples for two limiting cases.

Strong surface anisotropy, $K_{sur} \gg \sigma_{DW}$. In this case, $(\hat{Q}_I^{m-e} - \hat{Q}_{II}^{m-e}) \propto \lambda_{anis}/\mu$ and

$$\ell_{cr} = d_{opt} = \frac{\sigma_{DW}}{\lambda_{anis}^2/\mu} \propto \frac{\sigma_{DW}}{K_\perp} \propto \xi_{DW}. \tag{35}$$

Here we used the fact that the magnetic anisotropy in the AFM has the same nature as the magnetoelastic energy, resulting in $K_\perp \propto \lambda_{anis}^2/\mu$.

Weak surface anisotropy, $K_{sur} \gg \sigma_{DW}$. In this case $(\hat{Q}_I^{m-e} - \hat{Q}_{II}^{m-e}) \propto \lambda_{anis} K_{sur}/(\sigma_{DW}\mu)$, and so,

$$\ell_{cr} = d_{opt} = \frac{\sigma_{DW}}{\lambda_{anis}^2/\mu}\left(\frac{\sigma_{DW}}{K_{sur}}\right)^2 \propto \xi_{DW}\left(\frac{\sigma_{DW}}{K_{sur}}\right)^2 \gg \xi_{DW}. \quad (36)$$

Thus, in AFMs, as opposed to FMs, the domain size and the critical particle size depend on the properties of the surface (in this particular case – on the magnetic surface anisotropy). In the presence of strong surface anisotropy the characteristic size of the domain is of the same order of magnitude as the DW width. A similar result is obtained in the FMs, provided that the magnetic anisotropy is of the same order as the shape anisotropy. In the limiting case of zero surface magnetic anisotropy the critical particle size tends to infinity, in agreement with the expected absence of the shape effects in the large AFM samples (thermodynamic limit).

We emphasize that, in contrast to FMs, the equilibrium structure of AFMs is formed by the orientational domains only (the angle between vectors **L** in neighboring domains $< 180^\circ$). The translational 180° domains in collinear AFMs (that have opposite **L** directions) are physically indistinguishable and should be identified by the presence of the interfaces. This problem is out of the scope of the paper.

5. Domain structure of bulk samples

The above model predicts the occurrence of the domains in arbitrarily large (bulk) samples, provided that $K_{sur} \neq 0$. Contribution of the magnetoelastic charges to the surface energy is proportional to the sample volume and competes with the anisotropy energy in samples of any size. On the other hand, increasing the characteristic size of the sample, we can reduce the influence of surface on the local properties up to the thermodynamic limit. Thus, we can question the existence of the upper critical size, above which the sample can be considered as single-domain. To find a rigorous answer, we need to solve a complicated problem, which is beyond the scope of our work; we confine ourselves to a few physical considerations.

Formally, we may move to the case of physically large samples (to the thermodynamic limit) in two ways: either as $\lim_{K_{sur}\to 0} \lim_{\ell\to\infty}$, or in the other order $\lim_{\ell\to\infty} \lim_{K_{sur}\to 0}$. In the first case, the surface leads to the shape effects and the domain structure formation. Increasing the sample size, and thus the domain size, we obtain large homogeneous regions, in which the influence of domain walls and the surface can be neglected (this issue is discussed in detail below). In the second case, we exclude the surface from consideration and get the homogeneous throughout the sample solution (12), which corresponds to the energy minimum. The domain structure is absent and the size of the sample is not important as a thermodynamic parameter.

We emphasize that our estimates of the domain structure period (33) and lower critical sample size (34) are based on the simplified Kittel's model of striped domain structure with one characteristic period. While the optimal period is less than or equal to the critical sample size (34), such choice of seed distribution seems reasonable. However, if the sample size (and d_{opt}) increases, the contribution of the charges $\hat{Q}_{I,II}^{me}$ to the energy grows. At the same time, energy can be decreased by the branching (fractalization) of the domain structure: the surface of "large" domain stimulates formation of small domains inside. Similar structures were observed in ferromagnetic and ferroelastic materials (such as martensites, in which deformation is the primary order parameter [31]). In [32] authors show that the scale invariance of the two-dimensional Laplace equation causes the fractal nature of the ferromagnetic and intermediate state superconducting structures. In our case, assuming the Coulomb nature of the elastic forces, we can also expect that the system of Eqs. (18) contains a similar (probably more difficult) fractal solution. We suppose that a multi-domain hierarchical structure, which contains ever smaller regions with various orientations of the AFM vector, may also appear in large AFM samples. This leads us to the following conclusions.

First, for large ℓ we need to adjust the estimate (33) for the domain structure period d_{opt}. Indeed, the total length of the domain walls in the fractal structure increases with the domain size d as d^{D_H}, where D_H is the Hausdorf fractal dimension. Thus, the total energy of the domain walls changes as $w_{bound} \propto \ell d^{D_H-2}$ (similar estimate for multiferroic $BiFeO_3$ was made in [33]), and the optimal domain size is $d_{opt} \propto \ell^{1/(3-D_H)}$. For the striped domains $D_H = 1$, which yields (33); for branching structures, obviously, $D_H > 1$, and the dependence $d_{opt}(\ell)$ is stronger. Second, in the fractal structure the ratio of the surface energy to the bulk energy decreases with increasing ℓ slower than $1/\ell$, indicating the important role of the surface in large samples.

Finally, we note that branching domain structure also allows transition to thermodynamic limit: as we have already noted, for periodic structures the field of magnetoelastic charges is screened over distances of the order of d_{opt} from the surface. Thus, even in multidomain sample the local magnetic properties of homogeneous regions (such as orientation of AFM vector, AFMR frequencies, susceptibility, etc.) depend on the internal (bulk) parameters only, and the role of the surface energy is insignificant.

Let us discuss another, practical, approach to the concept of the upper critical dimension. Imagine that initially the multidomain sample is transferred to a single-domain, homogeneous state (without DWs) by an external field. The question is: will the domain structure appear after the field is switched off? As in the case of the FM materials, the answer depends on various parameters, including the size of the sample, and the magnitude of the DW formation activation barrier U_{bar}. As we have already noted, the domain formation starts at the surface – from edges or vertices of the particle, depending on the crystallographic orientation of the surface. The domain nucleus creates the elastic stress field; energy density of this field decreases with distance (in analogy with the elastic energy of dislocation field) as $[(Q^{me})^2/\mu]\ln r/r_0$ (r_0 is a characteristic size of the order of the nucleus curvature radius). If $U_{bar} > [(Q^{me})^2/\mu]$, then the domain walls preferably form in areas where the field of magnetoelastic charges located at the opposite edges add constructively. Hence, we estimate the upper critical size of the sample: $\ell_{cr}^{up} \propto r_0 \exp U_{bar}\mu/(Q^{me})^2$. In small particles, $\ell < \ell_{cr}^{up}$, the interaction of charges located at the opposite edges is sufficient for the DW formation. If $\ell > \ell_{cr}^{up}$, the sample may remain in the metastable single-domain state.

6. Discussion

We proposed the model that takes account of the magnetic surface anisotropy and magnetoelastic coupling and predicts the additional shape-dependent magnetic anisotropy in AFM. The surface anisotropy selects one of the easy magnetic axes as energetically favorable, while magnetoelastic long-range interactions transfer the influence of the surface on the entire NP bulk. Formally, the model describes such effects using the tensor of magnetoelastic charges (20) localized at the NP surface. The developed theory should appropriately describe the magnetic behavior of AFM particles with the pronounced magnetostriction, like NiO, α-Fe_2O_3 (hematite), Cr_2O_3, $LaFeO_3$, low-doped $La_{2-x}Sr_xCuO_4$, etc. (see Table 1). Moreover, analysis of various experiments with these materials gives clear evidences of different shape-induced effects which we discuss in this section.

Shape-induced magnetic anisotropy manifests itself in two ways: (i) as uniaxial anisotropy, which splits energy of otherwise degenerated equilibrium orientations of AFM vector; (ii) as a "demagnetizing" (destressing) factor, which promotes formation of a certain domain type.

The first effect occurs when the shape-imposed easy axis is perpendicular to the "proper" easy magnetic axis of the crystal (e.g., induced by an external magnetic field). The constants of intrinsic and shape-induced magnetic anisotropy are of opposite signs; so, there is a critical aspect ratio a/b, at which spin–flop transition of the AFM vector takes place. Such a behavior was observed in the rectangular-shaped stripes of $LaFeO_3$, in which the effective magnetic field was induced by the exchange coupling with underlying FM layer [10]. In particular, in the wide ($b=1$ μm) stripes with small aspect ratio the AFM vector was oriented along the field-defined easy magnetic axis, while in the thin ($b=200$ nm) stripes with the large aspect ratio AFM vector was parallel to the long edge of the sample, perpendicular to easy axis. At intermediate value $b\propto$ 500 nm (critical aspect ratio), the stripes demonstrated AFM domain structure that may originate due to the balance of shape-induced and proper magnetic anisotropies in the "spin-flop" point.

Correlation between the sample shape and effective magnetic anisotropy, K_{anis}, deduced from the spin-flop field values was established in the experiments [23,41]. Fig. 6 shows K_{anis} values for the elliptical Cr_2O_3 nanoparticles at different aspect ratios a/b [42] (down triangles). To validate the predictions of our model, we fit the experimental data (solid curve in Fig. 6) according to the expression

$$K_{\text{anis}}\left(\frac{a}{b}\right)=K^{(0)}_{\text{anis}}-2K^{\text{m-e}}J_1\left(\frac{a}{b}\right) \tag{37}$$

where $K^{(0)}_{\text{anis}}=7.8\times10^4$ erg/g can be treated as a "bare" magnetic anisotropy, $K^{\text{m-e}}=8.8\times10^4$ erg/g has magnetoelastic origin and $J_1(a/b)$ is a shape factor introduced in (25) (see also Eq. (28)).

Unexpectedly good agreement between calculated and measured dependencies [43] in Fig. 6 shows that for relatively large NP ($b\geq30$ nm) the main contribution to the shape effect arises from the flat sections of the surface (in this case shape factors $J_1(a/b)$ of the rectangular and elliptical particle are approximately the same).

The second effect appears when the domain structure is reversibly changed under the action of external fields (magnetic or mechanical). In the flat rectangular NP with $a\neq b$, the shape-induced anisotropy (see Eq. (31)) plays the same role as the external field, resulting in unbalance between the domains of different types. Reversible (or partly reversible) field-induced restructurization of the domain structure was observed in the bulk samples of different AFMs and discussed in our previous papers (see e.g. [14,44]). Here we would like to mention the shape memory effect in lightly doped $La_{2-x}Sr_xCuO_4$ [38] observed directly (as variation of the domain structure seen in polarized light) and indirectly (in magnetoresistance measurements). We believe that field-induced variation of the domain fraction in this case results from the competition between the destressing energy Eq. (31) and magnetic energy of the sample [45].

The constant of the surface anisotropy also determines the critical parameters limiting formation of the domain structure. For example, if the NP size is comparable with the domain structure period d, formation of the domain walls and thus of domain structure is unfavorable. On the other hand, for the elongated samples with $a\gg d$ but $|K_2^{\text{sh}}((a/b)_{\text{cr}})|\geq K_\perp$ (see (29)), there is only one possible equilibrium orientation of the AFM vector and thus only one type of domains. In this case, the orientation of the easy

Table 1
Parameters of AFM: u is magnetostriction, T_N is the Néel temperature (for bulk samples).

Crystal	u (10^{-5})	T_N (K)	Ref.
NiO	9	573	[34]
Cr_2O_3	2.8	308	[35]
$LaFeO_3$	23.8	738	[36,37]
$La_{2-x}Sr_xCuO_4$	1000	200	[38,39]
α-Fe_2O_3	$\propto 1$	250–260	[40]

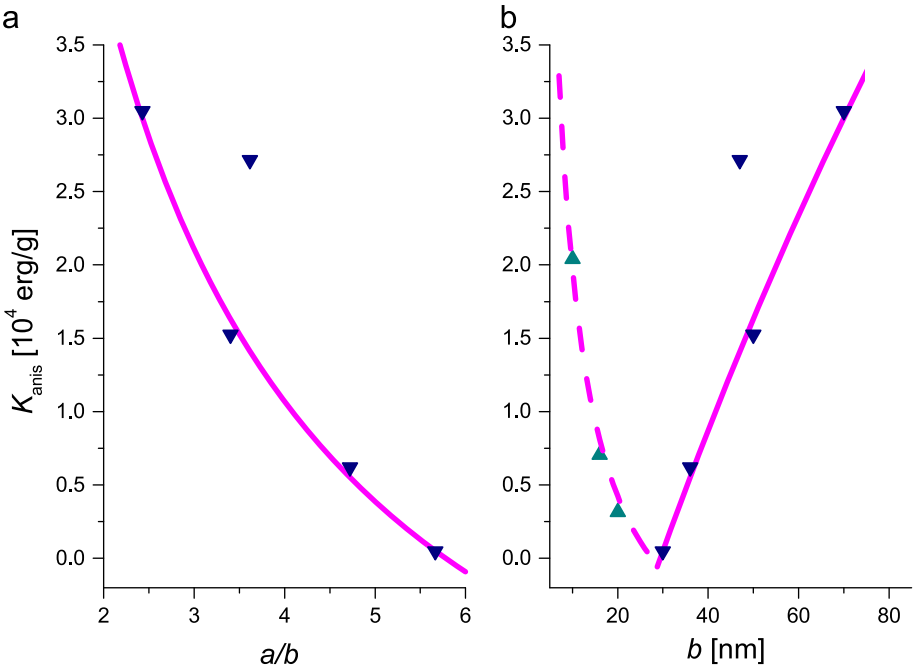

Fig. 6. Anisotropy constant of Cr_2O_3 nanoparticles as a function of (a) aspect ratio a/b; (b) minor size b. Down triangles show experimental data [23] for the elliptic particles with fixed $a=170$ nm, solid curve fits these data according to Eq. (37). Up triangles in the right panel (b) correspond to the experiments [41] with the spherical particles ($a=b$). Dashed line results from the linear fit of the inverse size dependence ($\propto 1/b$).

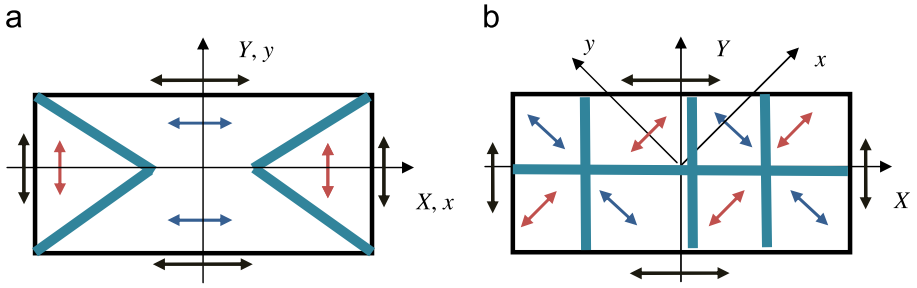

Fig. 7. Multidomain state of the nanoparticle with edges parallel (a) or at an angle 45° (b) relative to crystal axes. Arrows outside the rectangle indicate the orientation of the Néel vector at the surface.

axis depends not only on ratio a/b, but also on the angle ψ, which determines the orientations of the sample edges. So, the control of the AFM particles shape allows us not only to create single-domain samples, but also to drive the magnetic ordering direction.

The magnetoelastic charge-based formalism allows us to predict, at least qualitatively, the morphology of the domain structure depending on the size of the NP and crystallographic orientations of its edges. Note that charge contribution increases the energy density of NP compared with the case of an infinite crystal. So, charge-less (or zero mean) configuration is more favorable, as in FMs. If the NP edges are parallel to the crystallographic axes, the surface charges disappear in the structure that shown in Fig. 7a, – when the domain of a certain type grows from the edge into the bulk as far as possible. This type of the domain growth was observed experimentally in [12]; the authors named it "edge effect". Edge effect disappears if sample edges are rotated at angle $\psi = \pi/4$ with respect to easy magnetic axes. Really, in this geometry charge vanishes only in average (due to formation of the domain structure that is periodic along the edge, Fig. 7b). In this case, we assume that domain formation starts from the vertices of the rectangle, and the surface tension stresses can play a significant role in this process. A detailed discussion of this issue is beyond the scope of this paper.

The explicit form of the shape-induced anisotropy constants (28), (29) depends on the magnetic properties of the surface. In our model we suggest that the magnetic ordering at the surface somehow differs from that in the bulk, e.g. by orientation of easy axis (see (1)). However, it is possible to generalize the model and consider other typical situations: e.g., the surface of the sample is paramagnetic, unlike the bulk. In this case, we expect that the nonmagnetic shell will impose additional stresses (that result from incompatibility between magnetostriction of the core and zero strain at the surface) in the particle, which for large (multidomain) samples could show up in the destressing energy (similar to (31)). In the single-domain particles these stresses could result in the increase of the observed magnetostriction compared to the bulk samples, as it was experimentally found in NiO [1,46] and Cr_2O_3 [41] nanoparticles.

It is necessary to mention another contribution into shape-induced anisotropy ignored in our model. Namely, inhomogeneous distribution of AFM vectors (and/or elastic strains) at the surface can give rise to the "Laplas"-like stress proportional to the curvature of the surface. In the spherical-shaped particles the role of Laplas stress grows with a decrease of particle size. In particular, Fig. 6b illustrates this fact using as an example the size dependence of the effective anisotropy K_{anis} of small ($b \le 30$ nm) Cr_2O_3 particles. Experimental data [41] (up triangles) are rather well fitted with the inverse dependence $K_{\text{anis}} \propto 1/b$ (dashed curve). In the rectangular samples additional Laplas stresses may appear in the vicinity of the apexes.

Note that we have considered the ideal, i.e. defectless, sample, eliminating the energy of twin boundaries and disclinations (the latter inevitably arise in the areas of convergence of three or more domains), and neglecting peculiarities of the AFM vector distribution near the vertices of the rectangle. Certainly, these factors should influence the domain structure formation and the effective magnetic anisotropy of the sample. However, we assume that only the surface relates the internal magnetic properties of NP and its form. We have shown that the shape effects can be caused by the long-range fields of non-magnetic nature – elastic forces – and so they should appear in the "pure" AFM samples (without FM moment as well). The effects described above should be more pronounced in the small (up to few critical lengths) samples: in this case, the formation of the magnetic structure is determined mainly by the surface and the influence of the defects can be neglected.

The developed model can be applied to AFM particles whose dimensions are large enough to admit micromagnetic description. Typical thickness of the surface layer can be estimated as 1–3 nm (see, e.g., [47,48]), the minimal domain size observed in 12 nm particles of NiO was as small as 4 nm [49]. So, the model can describe, at least qualitatively, the particles even within the nanoscale range (i.e. 10–100 nm), however, below 100 nm the model should be generalized to account for the surface curvature, as explained above.

The proposed model is suitable for description of the bit-patterned media with AFM layer widely used in information technologies (see, e.g. [50–55]). Typical element has a submicron (down to 200 nm) size, rectangular shape and usually is well separated from the neighbors, so, it can be viewed as an alone-standing AFM particle considered above. On the other hand, such multilayered systems pose new interesting and nontrivial problems related to competition of shape effects resulted from both FM and AFM layers, interparticle interaction through the elastically soft substrate, etc.

In conclusion, the results obtained show that the shape can be used as a technological factor which allows us to drive, control and set the properties of antiferromagnetic nano- and submicron-sized samples.

The work is performed under the program of fundamental Research Department of Physics and Astronomy, National Academy of Sciences of Ukraine, and supported in part by a grant of Ministry of Education and Science of Ukraine (N 2466-f).

Appendix A. Green tensor method for the displacement field calculation

Assuming that we know the distribution of the AFM vector $\mathbf{L}(\mathbf{r})$, let us examine Eqs. (9)–(10) for the elastic subsystem. The corresponding boundary conditions at the surface are:

$$\frac{1+\nu_{\text{eff}}}{1-3\nu_{\text{eff}}}\mathbf{n}\,\text{div}\,\mathbf{u}+\begin{pmatrix} n_x(\nabla_x u_x-\nabla_y u_y)+n_y(\nabla_x u_y+\nabla_y u_x) \\ n_x(\nabla_x u_y+\nabla_y u_x)-n_y(\nabla_x u_x-\nabla_y u_y)\end{pmatrix} = -\frac{2\lambda_{\text{anis}}}{\mu}\mathbf{L}_{\text{sur}}(\mathbf{L}_{\text{sur}}\mathbf{n}). \quad (A.1)$$

To simplify, we skip the terms that describe the isotropic magnetostriction (as insignificant for further discussion).

We denote the bulk forces vector by

$$\mathbf{f} = -\begin{pmatrix} \nabla_x \cos 2\varphi + \nabla_y \sin 2\varphi \\ \nabla_x \sin 2\varphi - \nabla_y \cos 2\varphi \end{pmatrix}, \tag{A.2}$$

and the surface tension tensor (of the magnetostrictive nature) by $2(\lambda_{\text{anis}}/\mu)\mathbf{L}_{\text{sur}} \otimes \mathbf{L}_{\text{sur}}$.

Let the functions $G_{kj}(\mathbf{r},\mathbf{r}')$ $(k,j=x,y)$ be the solutions of the equation:

$$\Delta G_{kj}(\mathbf{r},\mathbf{r}') + \nu_{\text{eff}} \nabla_k \nabla_l G_{lj}(\mathbf{r},\mathbf{r}') = -\delta_{kj}\delta(\mathbf{r}-\mathbf{r}'), \tag{A.3}$$

with the following boundary conditions:

$$(\mathbf{n},\nabla) G_{kj}(\mathbf{r}_{\text{sur}},\mathbf{r}') + \nu_{\text{eff}}\left[n_k \nabla_l G_{lj}(\mathbf{r}_{\text{sur}},\mathbf{r}') + n_l \nabla_k G_{lj}(\mathbf{r}_{\text{sur}},\mathbf{r}')\right] = 0. \tag{A.4}$$

Here, δ_{kj} is the Kronecker symbol, $\delta(\mathbf{r}-\mathbf{r}')$ is the Dirac delta-function, $\mathbf{n}$ is the surface normal in point $\mathbf{r}_{\text{sur}}$.

The functions $G_{kj}(\mathbf{r},\mathbf{r}')$ coincide with Green tensor for isotropic medium with fixed stresses (accurate within constants). In this case, we can represent the displacement vector as follows:

$$u_j(\mathbf{r}) = -\frac{2\lambda_{\text{anis}}}{\mu}\int_V G_{kj}(\mathbf{r},\mathbf{r}')\nabla_l'[L_k(\mathbf{r}')L_l(\mathbf{r}')]\,dV' - \frac{2\lambda_{\text{anis}}}{\mu}\oint_S G_{kj}(\mathbf{r},\mathbf{r}_{\text{sur}}')L_k(\mathbf{r}_{\text{sur}}')L_l(\mathbf{r}_{\text{sur}}')\,dS_l' \tag{A.5}$$

Substituting (A.5) into energy expression (6) and taking into account boundary conditions (A.4), we obtain elastic and magnetoelastic energy contributions:

$$W_{\text{add}} = \frac{2\lambda_{\text{anis}}^2}{\mu}\int_V\int_V \nabla_m[L_j(\mathbf{r})L_m(\mathbf{r})]G_{kj}(\mathbf{r},\mathbf{r}')\nabla_l'[L_k(\mathbf{r}')L_l(\mathbf{r}')]\,dV\,dV' + \frac{2\lambda_{\text{anis}}^2}{\mu}\oint_S\oint_S L_j(\mathbf{r}_{\text{sur}})L_m(\mathbf{r}_{\text{sur}})G_{kj}(\mathbf{r}_{\text{sur}},\mathbf{r}_{\text{sur}}')L_k(\mathbf{r}_{\text{sur}}')L_l(\mathbf{r}_{\text{sur}}')\,dS_m\,dS_l'. \tag{A.6}$$

Appendix B. Shape-induced contribution into the magnetic energy for an arbitrary constant K_{sur}

In the general case, magnetoelastic charges (21) and (22) depend on the ratio $s \equiv \sigma_{DW}/K_{\text{sur}}$, which we took as a unit when obtained Eqs. (28) and (29). Here, we generalize these expressions for arbitrary values of s.

Substituting (21), (22) and (23), (24) into Eq. (8), we obtain expressions (27), where coefficients K_2^{sh}, K_4^{sh} depend on variables $\varphi^{(\text{in})}$:

$$K_2^{\text{sh}} = K^{\text{m-e}}\left[J_1\left(\frac{a}{b}\right)\frac{\Lambda_+ + \Lambda_-}{\Lambda_+\Lambda_-} - \left(1+\nu_{\text{eff}}J_2\left(\frac{a}{b}\right)\right)\frac{\Lambda_+ - \Lambda_-}{\Lambda_+\Lambda_-}\right], \tag{B.1}$$

$$K_4^{\text{sh}} = K^{\text{m-e}}\left[\left(2J_2\left(\frac{a}{b}\right)-1\right)\left(1-\frac{s(\Lambda_+ + \Lambda_-)}{2\Lambda_+\Lambda_-}\right) - J_1\left(\frac{a}{b}\right)\frac{s(\Lambda_+ - \Lambda_-)}{2\Lambda_+\Lambda_-}\right]. \tag{B.2}$$

Here,

$$\Lambda_\pm \equiv \sqrt{1 \pm 2s\,\cos\,2(\varphi_{\text{in}}+\psi)+s^2}. \tag{B.3}$$

In the limiting case of the small magnetic anisotropy ($s \gg 1$) both shape-dependent constants vanish:

$$K_2^{\text{sh}} = K^{\text{m-e}}J_1\left(\frac{a}{b}\right)\frac{2}{s} \to 0, \quad K_4^{\text{sh}} = -K^{\text{m-e}}J_1\left(\frac{a}{b}\right)\frac{\cos\,2(\varphi_{\text{in}}+\psi)}{s} \to 0. \tag{B.4}$$

Eq. (27) may perform as the minimum condition for the effective energy:

$$w_{\text{eff}} = -\frac{1}{4}K_\perp\,\cos\,4\varphi_{\text{in}} - \frac{1}{2s}K^{\text{m-e}}\left[J_1\left(\frac{a}{b}\right)(\Lambda_+ - \Lambda_-) + \left(1+\nu_{\text{eff}}J_2\left(\frac{a}{b}\right)\right)(\Lambda_+ + \Lambda_-)\right] - \frac{1}{12s}K^{\text{m-e}}\left[\left(2J_2\left(\frac{a}{b}\right)-1\right)\left(3\,s\cos\,4(\varphi_{\text{in}}+\psi) + 2(\Lambda_- + \Lambda_+)^3\right) - 2J_1\left(\frac{a}{b}\right)(\Lambda_- - \Lambda_+)^3\right]. \tag{B.5}$$

References

[1] M. Petrik, B. Harbrecht, in: 26 European Crystallographic Meeting Darmstard, Germany, 2010, pp. FA5–MS41–P11.
[2] M. Petrik, B. Harbrecht, Z. Kristallogr. Proc. 1 (2011) 253.
[3] X.G. Zheng, H. Kubozono, H. Yamada, K. Kato, Y. Ishiwata, C.N. Xu, Nat. Nanotechnol. 3 (2008) 724.
[4] M. Petrik, B. Harbrecht, Z. Anorgan. Allgem. Chem. 636 (2010) 2049.
[5] C. Bahl, L.T. Kuhn, K. Lefmann, P.-A. Lindgard, S. Morup, Phys. B: Condens. Matter 385–386 (1) (2006) 398.
[6] L. Néel, C.R. Hebd Séan. Acad. Sci. 328 (1949) 664.
[7] L. Néel, Low-temperature physics, in: C. de Witt, B. Dreyfus, P.-G. de Gennes (Eds.), Summer School of theoretical physics, les houches (1961) Théorie des propriétés magnétiques des grains fins antiferromagnétiques: superparamagnétisme et superantiferromagnétisme, Gordon & Breach, New York, New York, 1962, p. 413.
[8] R.H. Kodama, A.E. Berkowitz, E.J. McNiff Jr., S. Foner, Phys. Rev. Lett. 77 (1996) 394.
[9] S. Morup, C. Frandsen, F. Bodker, S.N. Klausen, K. Lefmann, P.-A. Lindgard, M.F. Hansen, in: P. Gutlich, B.W. Fitzsimmons, R. Ruffer, H. Spiering (Eds.), Mossbauer Spectroscopy, Springer, Netherlands, 2003, pp. 347–357.
[10] E. Folven, A. Scholl, S.T. Young, A. Retterer, J.E. Boschker, T. Tybell, Y. Takamura, J.K. Grepstad, Nano Lett. 12 (2012) 2386.
[11] E. Folven, A. Scholl, A. Young, S.T. Retterer, J.E. Boschker, T. Tybell, Y. Takamura, J.K. Grepstad, Phys. Rev. B 84 (2011) 220410.
[12] E. Folven, T. Tybell, A. Scholl, A. Young, S.T. Retterer, Y. Takamura, J.K. Grepstad, Nano Lett. 10 (2010) 4578.
[13] D.A. Garanin, H. Kachkachi, Phys. Rev. Lett. 90 (2003) 065504.
[14] H.V. Gomonay, V.M. Loktev, Phys. Rev. B 75 (2007) 174439.
[15] H. Gomonay, I. Kornienko, V. Loktev, Condens. Matter Phys. 13 (2010) 23701.
[16] M.I. Kaganov, Sov. Phys. JETP 52 (1980) 779.
[17] A.N. Bogdanov, U.K. Rößler, Phys. Rev. B 68 (2003) 012407.
[18] A.N. Bogdanov, U.K. Rößler, Phys. Rev. Lett. 87 (2001) 037203.
[19] A. Bogdanov, U. Rossler, K.-H. Muller, J. Magn. Magn. Mat. 238 (2002) 155.
[20] C. Kittel, Rev. Mod. Phys. 21 (1949) 541.
[21] N. Pérez, P. Guardia, A.G. Roca, M.P. Morales, C.J. Serna, O. Iglesias, F. Bartolomé, L.M. García, X. Batlle, A. Labarta, Nanotechnology 19 (2008) 5704.
[22] R.N. Bhowmik, R. Nagarajan, R. Ranganathan, Phys. Rev. B 69 (2004) 054430.
[23] D. Tobia, E. Winkler, R.D. Zysler, M. Granada, H.E. Troiani, Phys. Rev. B 78 (2008) 104412.
[24] L.D. Landau, E.M. Lifshits, 4th ed.,Theory of elasticity, course of theoretical physics, vol. 7, Fizmatgiz, Moscow, 1987, p. 246.
[25] S.K. Mishra, V. Subrahmanyam, Int. J. Mod. Phys. B 25 (2011) 2507.
[26] R.H. Kodama, S.A. Makhlouf, A.E. Berkowitz, Phys. Rev. Lett. 79 (1997) 1393.
[27] The values of the internal constants in NPs could differ significantly (by several times or even orders) from those for the bulk samples [1,3,56], where the role of the surface is negligible.
[28] V. Gann, A. Zhukov, Sov. Solid State Physics 22 (1980) 3188.
[29] E.A. Brener, V.I. Marchenko, Phys. Rev. Lett. 97 (2006) 067204.
[30] M. Petrik, B. Harbrecht, Solid State Phenom. 170 (2011) 244.
[31] M. Nishida, T. Hara, M. Matsuda, S. Ii, Mater. Sci. Eng.: A 481–482 (2008) 18.
[32] E.D. Belokolos, J. Phys. A: Math. General 34 (2001) 2331.
[33] G. Catalan, H. Béa, S. Fusil, M. Bibes, P. Paruch, A. Barthélémy, J.F. Scott, Phys. Rev. Lett. 100 (2008) 027602.
[34] T. Yamada, S. Saito, Y. Shimomura, J. Phys. Soc. Jpn. 21 (1966) 672.
[35] K.L. Dudko, V.V. Eremenko, L.M. Semenenko, Physica Status Solidi (b) 43 (1971) 471.
[36] S.C. Abrahams, R.L. Barns, J.L. Bernstei, Solid State Commun. 10 (1972) 379.
[37] D. Treves, J. Appl. Phys. 36 (1965).
[38] A.N. Lavrov, S. Komiya, Y. Ando, Nature 418 (2002) 385.
[39] A. Nabialek, P. Komorowski, M.U. Gutowska, M.A. Balbashov, J.N. G?recka, H. Szymczak, O.A. Mironov, Supercond. Sci. Technol. 10 (1997) 786.
[40] R.A. Voskanya, R.Z. Levitin, V.A. Shchurov, Sov. Phys. JETP 27 (1968) 423.
[41] D. Tobia, E. De Biasi, M. Granada, H.E. Troiani, G. Zampieri, E. Winkler, R.D. Zysler, J. Appl. Phys. 108 (2010) 104303.
[42] Originally, in [23] K_{anis} was measured as a function of synthesis temperature whose value correlates with the minor size b of the nanoparticles. The major axis kept approximately constant value 170 nm.
[43] At large $b \to a$ the particle can split into multidomain state. In this case approximation (37) should be corrected.
[44] E.V. Gomonaj, V.M. Loktev, Phys. Rev. B 64 (2001) 064406.

[45] In the experiments [38] shape memory effect was observed below and above the Néel point. In the latter case expression for destressing energy should be written in terms of strains, not AFM vectors.
[46] M. Petrik, B. Harbrecht, Z. Anorgan. Allgem. Chem. 634 (2008) 2069.
[47] J. Ma, K. Chen, Phys. Lett. A 377 (2013) 2216.
[48] J.F.K. Cooper, A. Ionescu, R.M. Langford, K.R.A. Ziebeck, C.H.W. Barnes, R. Gruar, C. Tighe, J.A. Darr, N.T.K. Thanh, B. Ouladdiaf, J. Appl. Phys. 114 (2013) 083906.
[49] S. Klausen, P.-A. Lindgard, K. Lefmann, F. Bodker, S. Morup, Phys. Status Solidi A 189 (2002) 1039.
[50] A. Moser, K. Takano, D.T. Margulies, M. Albrecht, Y. Sonobe, Y. Ikeda, S. Sun, E.E. Fullerton, J. Phys. D: Appl. Phys. 35 (2002) R157.
[51] S. Maat, K. Takano, S.S.P. Parkin, E.E. Fullerton, Phys. Rev. Lett. 87 (2001) 087202.
[52] Y. Takamura, R.V. Chopdekar, A. Scholl, A. Doran, J.A. Liddle, B. Harteneck, Y. Suzuki, Nano Lett. 6 (2006) 1287.
[53] I.L. Prejbeanu, S. Bandiera, J. Alvarez-Hérault, R.C. Sousa, B. Dieny, J.-P. Nozíres, J. Phys. D: Appl. Phys. 46 (2013) 074002.
[54] T. Hasegawa, T. Tomioka, Y. Kondo, H. Yamane, S. Ishio, J. Appl. Phys. 111 (2012) 07.
[55] A.D. Lamirand, M.M. Soares, A.Y. Ramos, H.C.N. Tolentino, M. De Santis, J.C. Cezar, A. de Siervo, M. Jamet, Phys. Rev. B 88 (2013) 140401.
[56] Z.H. Sun, X.Y. Song, F.X. Yin, L.X. Sun, X.K. Yuan, X.M. Liu, J. Phys. D: Appl. Phys. 42 (2009) 122004.